We are IntechOpen,
the world's leading publisher of
Open Access books
Built by scientists, for scientists

6,900
Open access books available

185,000
International authors and editors

200M
Downloads

154
Countries delivered to

Our authors are among the

TOP 1%
most cited scientists

12.2%
Contributors from top 500 universities

CLARIVATE ANALYTICS
**BOOK
CITATION
INDEX**
INDEXED

WEB OF SCIENCE™

Selection of our books indexed in the Book Citation Index
in Web of Science™ Core Collection (BKCI)

Interested in publishing with us?
Contact book.department@intechopen.com

Numbers displayed above are based on latest data collected.
For more information visit www.intechopen.com

Dynamic Testing of Data Acquisition Channels Using the Multiple Coherence Function

Troy C. Richards

Additional information is available at the end of the chapter

http://dx.doi.org/10.5772/48539

1. Introduction

The use of the Fast Fourier Transform (FFT) has revolutionized digital signal processing in many ways; and one of its principle uses continues to be the calculation of power spectral densities that are then used to estimate system transfer functions. When performing transfer function measurements, best practise dictates that the coherence between the input and output also be computed to provide a measure of the confidence in the measurement.

Many researchers, however, have turned the FFT based calculation of system transfer functions into a means to identify and remove coherent noise present in sensor measurements. Based on power spectral densities calculated using the FFT, the coherent noise between signals can be determined and then subtracted to reduce the noise floor of the sensor data acquisition channel.

To achieve good coherence between the input and output signals at all frequencies of interest it is necessary to ensure that those frequencies are present in the input signal. Poor coherence between the input and output can identify frequencies where external signals are being picked up, or it can indicate that the input or output signals are reduced or not present. Good coherence at all frequencies of interest can only be achieved with the use of white or wideband input noise signals.

When the dynamic range of the device under test exceeds that of the measuring device, over the frequency range of interest, maintaining good coherence becomes increasingly difficult. In these cases, it becomes necessary to use band-limited inputs, or sine wave inputs, where the signal gains can be optimized to improve the dynamic range and the coherence.

Manufacturers and end-users alike require methods to characterize the performance or quality of the data acquisition channels they either produce or use. The study of quality, however, is actually devoted to understanding the noise of the devices under test. Often manufacturers report zero-input noise levels for their devices, however, those levels may not be achieved when the device is performing during actual use. The coherent removal procedure, to be

presented, provides a method to dynamically test amplifiers, filters, or analog-to-digital (A/D) converters, and to compute their noise levels when using typical input signals.

The idea of inputting a white noise signal into two A/D converters and computing the residual spectra from the ordinary coherence function, in order to characterize the noise of the devices was first reported in [19], and that concept was extended to testing multiple A/D converters using the multiple coherence function in [20]. In this chapter, those methods are expanded to encompass the entire data acquisition channel, so that dynamic testing of multiple amplifiers, filters or A/D converters can be performed.

1.1. Preface

Bendat and Piersol's texts [1, 2] provide much of the theoretical background to the work to be presented here. Their treatment of the subject matter walks the reader through power spectral density estimation with discrete Fourier transforms and introduces data windowing and averaging periodograms, to arrive at estimates of the auto power spectral density based on the method popularized by Welch [21]. The foundation for both single-input single-output systems, as well as multiple-input single-output systems is also established, as is the concept of the coherent estimate of the output signal, and the residual spectrum.

The removal of coherent background signals is particularly effective at improving detection ranges of electromagnetic (EM) sensing systems, where incoming background micro-pulsation EM signals arrive virtually instantaneously on remote sensors (known as reference sensors), and can be (coherently) subtracted from signals monitoring areas of interest [6, 10, 17]. The removal of coherent background signals lowers the noise floor and therefore increases the detection range of the EM sensing system.

In the early efforts of using the multiple coherent removal procedure to enhance array performance, the number of reference sensors was limited to two or three channels and the required equations were solved for the given case. Recognizing that the system of equations for the optimum system transfer functions gave rise to a positive definite matrix which could be solved using the Cholesky algorithm was first reported in [20]. (Although, the conditioned spectral densities discussed by Bendat and Piersol bare close resemblance to the Cholesky decomposition into a lower triangle matrix, known as the square root of the matrix, followed by the back substitution procedure to yield the solution.) This approach then allowed any number of channels to be easily and efficiently programmed and solved. In that same work, the level of the residual spectrum was interpreted in terms of the noise of the individual A/D converters and a procedure was given to compute the individual A/D converter noise levels.

The IEEE has recently approved a standard [8] on the terminology and testing of A/D converters to provide a framework on the reporting on the dynamic testing of A/D converters. All of the principle methods discussed; the frequency domain method, the curve-fit method and the histogram method, use sine waves for their input signal. As the quality of the devices under test has improved, so too have the requirements for the spectral purity of the sine wave and the requirement to synchronize the sine wave frequency with the sampling rate. The frequency domain method has emerged as the most commonly used technique, however with the increasing resolution of A/D converters this approach will be limited by spectral leakage even for the best data windows. For end users who wish to verify the advertised specifications

of high quality devices, the requirements of the test signal can be difficult and expensive to attain, in that, a standard off-the-shelf function generator is insufficient to perform the testing.

The relationship between coherence and time delay has been extensively studied, and the selected IEEE reprint volume [5] is an excellent reference on the subject (the single-input single-output treatment given here parallels page 1 of that work very closely). One of the most significant results in the volume is provided by Carter [4] where it is shown that the coherence function, as calculated using the FFT, has a bias error proportional to the delay between the signals.

It is, precisely the reason, that the coherence function as estimated using the FFT method, is biased by the time delay between those signals, which results in rather poor performance when attempting to remove coherent background acoustic signals. Sound waves travel much slower then EM waves and, therefore, there can be appreciable delay between the arrival of background acoustic signals.

The coherent removal technique is, however, well suited to testing multiple data acquisition channels because, generally, it is a simple matter to synchronize signals under user control. Simultaneously sampling the inputs is one of the basic principles behind the success of FFT-based spectrum analyzers.

1.2. Chapter overview

The chapter begins with a brief review of Welch's procedure for estimating the auto and cross power spectral densities of signals, and introduces the concept of determining the root mean square (rms) level of a signal in the frequency domain. Next the single-input single-output system and optimum system transfer function is introduced, and the concept of the coherent output and residual spectrum is explained. These results are then generalized for the multiple-input single-output system. Procedures for computing the cross spectral densities of a general number of signals are then discussed and the solution of the optimum system transfer functions using the Cholesky decomposition is presented, to establish the background theoretical material for the remainder of the chapter.

Next a general model for a data acquisition channel is introduced, which includes both amplifier and A/D converter noise sources, along with an noiseless gain and filter stage. To interpret the residual spectrum where any number of channels are tested, each channel of a multiple-input single-output system is represented by the data acquisition channel model, and the optimum system transfer functions and residual spectrum are determined in terms of the data acquisition model parameters. These results are then generalized, to allow any of the channels to be the output and the remaining channels the inputs. Assuming the input signal is large and the channel characteristics are matched leads to simple expressions for the optimum system transfer functions and the residual spectra, in terms of the data acquisition channel model parameters. It is then demonstrated how to test for either the amplifier noise or the A/D converter noise of the acquisition channel by adjusting the channel gain.

Measurement examples are then given demonstrating the technique with a set of analog amplifiers and filters, measured with simultaneously-sampled, 24-bit, sigma-delta ($\Delta\Sigma$) A/D converters, as well as a 16-bit, multiplexed, successive approximation register (SAR) A/D converter, with a constant inter channel delay between channel samples.

Firstly, the well-accepted procedure of using the FFT to compute the (single-input single-output) transfer functions is demonstrated by computing the transfer functions for each of the amplifiers and filters under test. Next, the multiple coherent removal procedure is used to calculate the noise of the high resolution $\Delta\Sigma$ A/D converters, and then the SAR-based A/D converter, using a wideband noise source, and then a narrower band noise source. Results are then presented for the noise of the amplifiers under test using the same inputs. The final measurement examines the implications of using a sine wave as the test signal, and the effect of data windowing is examined. Lastly, a brief summary of the presented work, highlighting areas of interest, is given.

2. Basic definitions of coherent removal

2.1. Calculation of the power spectral density

Generalizing the procedure made popular by Welch [21] for computing the power spectral density of one signal, the cross spectral density of two signals can be estimated by averaging the product of the FFT of segments of the two signals. If x and y represent the two data streams, and X_k and Y_k are the FFT of the k-th segment of data, which is possibly overlapped and windowed (to enhance its spectral content), the cross spectral density can be estimated as the average of K segments and is given as

$$S_{xy} = \frac{1}{KU} \sum_{k=1}^{K} X_k^* Y_k,$$ (1)

where * denotes the complex conjugate, and the quantity

$$U = f_s \sum_{n=1}^{M} w(n)^2$$ (2)

is a constant which accounts for the spectral weighting of the data window $w(n)$ and, assuming the input is measured in volts, properly scales the power spectral density to have units of a volts squared per hertz (V^2/Hz). The segment length, which is also equivalent to the window length is defined as M, and the FFT size is defined as P, which is typically a power of 2 and is greater than M.

The auto (or self) spectral density, can be determine by setting $x = y$ to arrive at

$$S_{xx} = \frac{1}{KU} \sum_{k=1}^{K} |X_k|^2.$$ (3)

As is evident by the above expressions the auto spectral densities are real valued, whereas, cross spectral densities are complex-valued functions.

Using Parseval's theorem, the root mean square (rms) level of the signal x, defined as σ_x, can be estimated as

$$\sigma_x^2 = \frac{f_s}{P} \sum S_{xx},$$ (4)

where f_s is the sampling rate. The rms level calculated by Equation (4) is an averaged quantity and will be approximately equal to the variance of the (entire) signal computed in the time

domain. (For each individual segment the computation of the rms level in the time and frequency domains are precisely equal, as required by Parseval's theorem.)

Some references explicitly define both a one-sided and two-sided spectral density, while the definitions used here are not specific to either definition, when plotting spectral densities we shall use the accepted practise of plotting the one-sided spectral density, so that the spectral density values are doubled and one side of the spectra plotted. By this approach, summing the $P/2$ values of the one-sided spectral of density, will yield the rms level of x as defined in Equation (4). It is helpful to consider the operation as a numeric integration of the spectral density, so that S_{xx} is summed over all frequency bins and then multiplied by the integration width fs/P, to obtain the square of the rms level σ_x^2.

The use of the Welch FFT-based method for computing spectral densities is well documented in the literature, the texts by Kay [9] and Marple [11], and their review paper [12], as well as the text by Oppenheim and Schafer [16], all have sections devoted to the Welch method. In MATLAB, the Signal Processing Toolbox includes the functions `pwelch` and `cpsd` for calculating auto and cross spectral densities [14]. In Section 2.5 of this chapter the Welch procedure is generalized for any number of signals.

2.2. Single-input single-output systems

A common use of spectral densities estimated by the Welch method is to compute the transfer function of an amplifier or filter under test. Digitally recorded representations of the input signal x and output signal y of a device can be segmented, possibly overlapped, windowed to improve spectral content, and the spectral densities S_{xx}, S_{yy} and S_{xy} calculated. The optimum system transfer function, in terms of its expected value or minimizing the error between y and the output of the filter, is given as

$$H_{xy} = \frac{S_{xy}}{S_{xx}}. \tag{5}$$

The coherence between the two signals, is defined as

$$C_{xy} = \gamma_{xy}^2 = \frac{\left|S_{xy}\right|^2}{S_{xx}S_{yy}} \tag{6}$$

and is a measure of how well the two signals are linearly related to each other. The coherence function is normalized such that $0 \leq C_{xy} \leq 1$. Good coherence, $C_{xy} \approx 1$, is essential to accepting the calculation of H_{xy} as the true transfer function of the device under test. The coherence function between just two channels, is sometimes referred to as the *ordinary coherence function*. The calculation of frequency domain transfer functions based on Welch's procedure and ultimately the FFT, forms the computational basis of many two-channel spectrum analyzers.

2.3. Concept of coherent removal

To understand the concept of coherent removal it is useful to refer to the single-input, single-output model in Fig. 1, and to define v as the signal at the output of H_{xy}. Since the optimum system transfer function, in terms of its expected value or minimizing the square
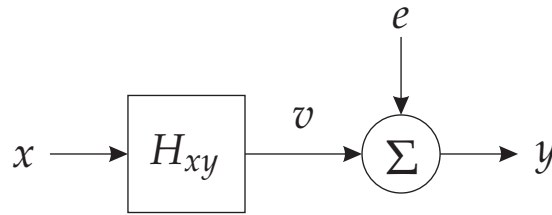
Figure 1. Single-input single-output system where H_{xy} is the optimum transfer functions which linearly relate the input x to the system system output y.

of the error signal e, is given by Equation (5), the spectral density of v can be equivalently expressed as

$$S_{vv} = |H_{xy}|^2 S_{xx} = H_{xy}^* S_{xy} = C_{xy} S_{yy} \tag{7}$$

and is recognized as the portion of y, which can be linearly accounted for by the input x.

Also, as a consequence of the optimization procedure, the error signal is uncorrelated with S_{vv}, and therefore, the power spectral density of the output can be written as

$$S_{yy} = S_{vv} + S_{ee}. \tag{8}$$

The error, or residual spectral density, is then given as

$$S_{ee} = S_{yy} - S_{vv} = S_{yy}\left(1 - C_{xy}\right), \tag{9}$$

and represents the portion of y, which is not linearly accounted for by the input x. In practise, since the spectral density of the error signal, S_{ee}, is always greater than zero, S_{vv} is always less than S_{yy}.

On rearrangement of Equation (9), the signal to residual noise ratio can be determined as

$$\frac{S_{yy}}{S_{ee}} = \frac{1}{1 - C_{xy}}. \tag{10}$$

This ratio is often termed the degree of cancellation and for coherent removal applications provides a useful measure of the coherence and is an important indicator of the quality of the measurement. Since larger input signals, increase the value of the signal to residual noise ratio, it should be quoted along with the input signal level. For the spectral density plots presented later, one can easily estimate the degree of cancellation in dB by subtracting the level of the input signal from the residual spectrum.

The residual spectrum is computed directly from the recorded data and can always be calculated regardless of the data set. In a worse case scenario, where the input signal is completely uncorrelated with the output, the residual spectra would be equal to the output spectrum and S_{vv} would be zero. Conversely, perfect coherence of unity is only achieved when the signals are identical and then Equation (10) approaches infinity. To avoid this possibility, it is sometimes advantageous to add random noise to each channel at a level sufficient to ensure that the inputs are not equal but small enough not to impact the results. Such measures are ordinarily not required as there is usually sufficient difference in the signals being processed.
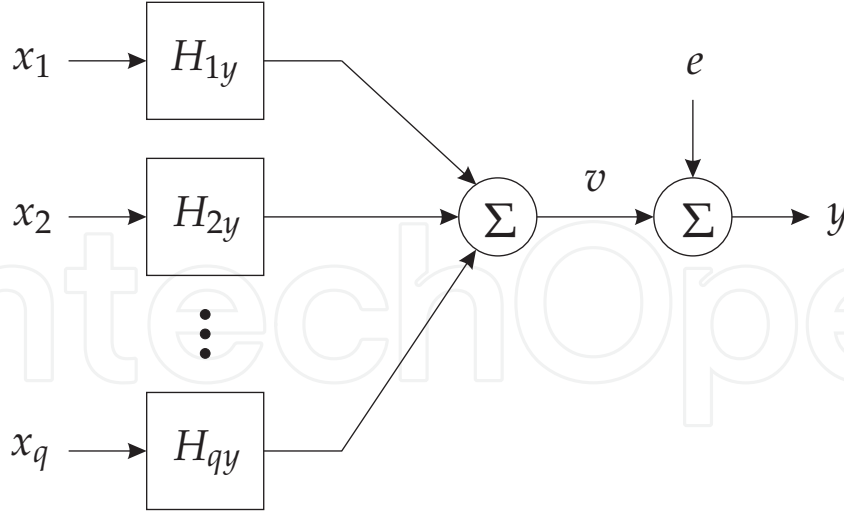
Figure 2. Multiple-input single-output system where $\{H_{iy}, i = 1\dots q\}$ are the optimum system transfer functions which linearly relate the inputs $\{x_i, i = 1\dots q\}$ to the system system output y.

2.4. Multiple-input single-output systems

To expand the single channel coherent removal concept to the multiple channel case, consider the system shown in Fig. 2, where the q inputs $\{x_i, i = 1, \dots, q\}$ and the output signal y, are measured signals and the goal is to determine the optimum transfer functions $\{H_{iy}, i = 1, \dots, q\}$ which best relate the inputs to the output. Representing the $\mathcal{Z}$-transform of a signal by its upper case, the operations depicted in Fig. 2 can be described as

$$Y = V + E = \sum_{i=1}^{q} H_{iy} X_i + E, \tag{11}$$

where v is the optimum estimate of y, and e is the error between the two signals.

The optimum system transfer functions which minimize the error, can be determined in a least squares or an expected value sense, and are given by the solution of the following equations [2, Eq.(8.12)],

$$S_{iy} = \sum_{j=1}^{q} H_{jy} S_{ij} \quad \text{for} \quad i = 1, \dots, q, \tag{12}$$

where $S_{ij} = S_{x_i x_j}$, represents the cross spectral density of x_i and x_j, and $S_{iy} = S_{x_i y}$ is the cross spectral density of x_i and the output y. To appreciate the structure of these equations it is useful to express them in matrix form as:

$$\begin{bmatrix} S_{1y} \\ S_{2y} \\ \vdots \\ S_{qy} \end{bmatrix} = \begin{bmatrix} S_{11} & S_{12} & \cdots & S_{1q} \\ S_{21} & S_{22} & \cdots & S_{2q} \\ \vdots & \vdots & \ddots & \vdots \\ S_{q1} & S_{q2} & \cdots & S_{qq} \end{bmatrix} \begin{bmatrix} H_{1y} \\ H_{2y} \\ \vdots \\ H_{qy} \end{bmatrix}. \tag{13}$$

Noting that $S_{ij} = S_{ji}^*$, the square matrix in Equation (13) is recognized as being positive definite, and therefore, the equations can be efficiently solved using the Cholesky decomposition.

The Cholesky decomposition separates a positive definite matrix into the product of a lower triangle matrix and its conjugate transpose. The resulting lower triangle matrix is sometimes referred to as the square root of the matrix, and once determined allows the equations to be solved using the back substitution method. Numerical procedures for the Cholesky decomposition are discussed in [18]. With an FFT size of P, the optimum system transfer functions will require the solution of $P/2$ sets of q simultaneous equations. Using the Cholesky decomposition for each set of these equations provides the most efficient, as well as accurate solution.

Once the optimum transfer functions are determined, the power spectral density of the best linear predictor due to the q inputs can be calculated from [2, Eq.(8.36)] as

$$S_{vv} = \sum_{i=1}^{q} H_{iy}^* S_{iy} \tag{14}$$

$$= H_{1y}^* S_{1y} + H_{2y}^* S_{2y} + \cdots + H_{qy}^* S_{qy}. \tag{15}$$

Similar to the single input case, the error spectral density is given as

$$S_{ee} = S_{yy} - S_{vv} = S_{yy} \left(1 - C_{\mathbf{x}:y}\right), \tag{16}$$

and represents the portion of y, which is not linearly accounted for by the multiple inputs, in this case. And, here, the multiple coherence function has been introduced, and is defined as

$$C_{\mathbf{x}:y} = \frac{S_{vv}}{S_{yy}}. \tag{17}$$

For the dynamic testing of acquisition channels, the primary interest is actually the residual spectrum, and therefore the multiple coherence function often remains uncalculated.

2.5. Calculation of the cross power spectral density for multiple channels

To obtain the required cross spectral densities used to calculate the optimum system transfer functions, and ultimately the residual spectrum, the Welch spectral estimates must be computed for all auto and cross spectral densities of the inputs and the output.

To accomplish this task, each time segment of the q input channels and the output channel can be arranged into a matrix defined as

$$\boldsymbol{x}_k = \left(\begin{bmatrix} \\ x_1 \\ \\ \end{bmatrix}_k \begin{bmatrix} \\ x_2 \\ \\ \end{bmatrix}_k \cdots \begin{bmatrix} \\ x_q \\ \\ \end{bmatrix}_k \begin{bmatrix} \\ y \\ \\ \end{bmatrix}_k \right) \tag{18}$$

where $[x_i]_k$ is a column vector of the k-th time segment of the i-th channel. Performing the FFT on each column of the $\boldsymbol{x}_k$ matrix produces the FFT matrix of $\boldsymbol{x}_k$ defined as

$$\boldsymbol{X}_k = \left(\begin{bmatrix} \\ X_1 \\ \\ \end{bmatrix}_k \begin{bmatrix} \\ X_2 \\ \\ \end{bmatrix}_k \cdots \begin{bmatrix} \\ X_q \\ \\ \end{bmatrix}_k \begin{bmatrix} \\ Y \\ \\ \end{bmatrix}_k \right). \tag{19}$$

To construct the cross, and auto, spectra of all channels, each row of X_k can be extracted and multiplied by its conjugate transpose, in an operation often referred to as the outer product.

To explicitly recognize the frequency dependence each row of X_k can be identified as $X_k(f)$, then, to obtain the cross spectral densities, the outer products are averaged for each of the K data segments, to yield the cross spectral density matrix, which can now be expressed as

$$S_{ij}(f) = \frac{1}{KU} \sum_{k=1}^{K} X_k^H(f) X_k(f) \tag{20}$$

$$= \begin{bmatrix} S_{11} & S_{12} & \cdots & S_{1q} & S_{1y} \\ S_{21} & S_{22} & \cdots & S_{2q} & S_{2y} \\ \vdots & \vdots & \ddots & \vdots & \vdots \\ S_{q1} & S_{q2} & \cdots & S_{qq} & S_{qy} \\ S_{y1} & S_{y2} & \cdots & S_{yq} & S_{yy} \end{bmatrix}. \tag{21}$$

Where ^{H} represents the conjugate transpose, and the explicit reference to the frequency dependence of the cross spectral densities has been omitted. The matrix S_{ij}, now contains all the elements required to calculate the optimum system transfer functions in Equation (13), the optimum predictor S_{vv} given in Equation (15), and the residual spectrum S_{ee} in Equation (16).

3. Applying coherent removal to testing acquisition channels

With the ability to remove the coherent or linear portion of a signal, it is now possible to suppress coherent noise signals, and this is how the technique is used to improve the detection ranges of EM sensing systems. It is also possible to use the procedure to dynamically test sensors, amplifiers and A/D converters by applying the same signal to multiple devices under test and remove the coherent portion based on multiple channel recordings. The difficulty arises in interpreting what the residual error means in terms of the noise of the devices under test. To answer this question, one must first define a noise model for a single data acquisition channel, and then determine the optimum system transfer functions and residual spectrum, in terms of the data acquisition model parameters of each channel.

3.1. Data acquisition channel noise model

In the study of noise in electronic components, it is usual to lump together all noise sources into equivalent noise sources for the whole device [15]. Assuming that multiple acquisition channels are operating, Fig. 3 considers the i-th channel which is sampling some input signal u_i and the system output x_i is a digital representation of u_i. The additive input noise m_i is met to represent the amplifier noise, while the additive output noise source n_i represents the quantization noise or A/D converter noise. The channel transfer function G_i relates u_i to x_i and takes into account gain and anti-aliasing requirements of the data acquisition channel.

Assuming that m_i and n_i are uncorrelated with each other and the input u_i, we can write the auto spectral density of x_i as

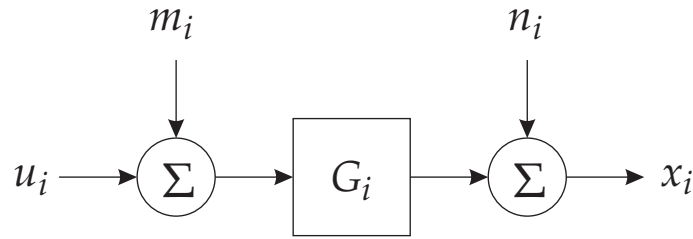$$S_{ii} = |G_i|^2 (S_{u_i u_i} + S_{m_i m_i}) + S_{n_i n_i}. \tag{22}$$

Figure 3. Equivalent noise model of a data acquisition channel, where x_i is the digitally recorded representation of the true input signal u_i. The additive noise sources, m_i and n_i represent the amplifier noise and converter noise, respectively, and the ideal linear transfer function G_i takes into account gain and anti-aliasing requirements.

If we now consider a second channel x_j and assume that its noise sources m_j and n_j are uncorrelated with each other and the inputs x_i and x_j, we can write for the cross spectral density of x_i and x_j, that

$$S_{ij} = G_i^* G_j \left(S_{u_i u_j} + S_{m_i m_j} \right) + S_{n_i n_j}. \tag{23}$$

3.1.1. Zero-input noise level

When the input signal is zero, the auto spectral density of the output becomes the zero-input noise level and is given as

$$S_{ii} = |G_i|^2 S_{m_i m_i} + S_{n_i n_i}. \tag{24}$$

This term represents all the noise present in the acquisition channel and is sometimes referred to as the combined noise. As a rule, when performing noise measurements the gain of the channel is adjusted to test for the noise of the amplifier or the converter, separately.

3.2. Interpretation of the residual spectrum

In [20] the residual spectrum was interpreted for the case where the A/D converter noise is dominate over the gained amplifier noise. To determine a more general result, in terms of both the amplifier and converter noise sources, we can substitute the expressions given in Equations (22) and (23) into Equation (12), to obtain the following general expression for the optimum system transfer functions

$$G_i^* G_{q+1} \left(S_{u_i u_{q+1}} + S_{m_i m_{q+1}} \right) + S_{n_i n_{q+1}} = \sum_{j=1}^{q} H_{jy} \left(G_i^* G_j \left(S_{u_i u_j} + S_{m_i m_j} \right) + S_{n_i n_j} \right), \tag{25}$$

where the output channel y, is identified as the $q+1$ data acquisition channel. To this point, the only assumption made is that the true signals u_i are uncorrelated with the noise sources n_i and m_i. These equations allow for individual amplifier and converter noise levels, for correlation to exist between the noise sources, and include the effects of the gain and anti-aliasing filters.

3.2.1. Uncorrelated noise approximation

Electronic devices which are manufactured and packaged together will have similar noise characteristics. Nevertheless, when physically isolated from one another or when operating

independent of each other, no linear relationship will exist between the instantaneous noise values and therefore, the noise, although similar, will be uncorrelated. When multiple data acquisition channels are used in a common operating environment some correlation will undoubtedly exist between the equivalent noise sources, however, very often it is possible to assume with little error, that the noise sources under consideration are uncorrelated [15, p.24].

Applying this basic underlying assumption of the study of noise to our example, if the noise sources are uncorrelated with each other then $S_{m_i m_j} = 0$ and $S_{n_i n_j} = 0$ for $i \neq j$, and Equation (25) will simplify to

$$G_i^* G_{q+1} S_{u_i u_{q+1}} = H_{iy} \left(|G_i|^2 S_{m_i m_i} + S_{n_i n_i} \right) + \sum_{j=1}^{q} H_{jy} G_i^* G_j S_{u_i u_j}. \tag{26}$$

To proceed, it becomes necessary at this point to enforce that all the inputs are the same signal, so that $u = u_i = u_{q+1}$, which allows us to divide through by S_{uu}, to arrive at

$$G_i^* G_{q+1} = H_{iy} \frac{|G_i|^2 S_{m_i m_i} + S_{n_i n_i}}{S_{uu}} + \sum_{j=1}^{q} H_{jy} G_i^* G_j. \tag{27}$$

The structure of these equations is, perhaps, better demonstrated in matrix notation as:

$$\begin{bmatrix} G_1^* \\ \vdots \\ G_q^* \end{bmatrix} G_{q+1} = \left(\begin{bmatrix} \frac{|G_1|^2 S_{m_1 m_1} + S_{n_1 n_1}}{S_{uu}} & 0 & 0 \\ 0 & \ddots & 0 \\ 0 & 0 & \frac{|G_q|^2 S_{m_q m_q} + S_{n_q n_q}}{S_{uu}} \end{bmatrix} + \begin{bmatrix} G_1^* \\ \vdots \\ G_q^* \end{bmatrix} \begin{bmatrix} G_1 & \cdots & G_q \end{bmatrix} \right) \begin{bmatrix} H_{1y} \\ \vdots \\ H_{qy} \end{bmatrix}, \tag{28}$$

where it is now observed that the solution requires the inversion of a matrix which is the sum of a diagonal matrix and an outer product.[1] Computing the inverse of this matrix, one arrives at the solution for the optimum system transfer functions in terms of the data acquisition channel parameters, given as

$$H_{iy} = \frac{G_i^* G_{q+1} S_{uu}}{|G_i|^2 S_{m_i m_i} + S_{n_i n_i}} \left(1 + \sum_{k=1}^{q} \frac{|G_k|^2 S_{uu}}{|G_k|^2 S_{m_k m_k} + S_{n_k n_k}} \right)^{-1}. \tag{29}$$

Substitution of this result into Equation (15), and then into Equation (16), leads to an expression for the residual error in terms of the data acquisition channel parameters, which is given as

$$S_{ee} = |G_{q+1}|^2 S_{m_{q+1} m_{q+1}} + S_{n_{q+1} n_{q+1}} + |G_{q+1}|^2 S_{uu} \left(1 + \sum_{k=1}^{q} \frac{|G_k|^2 S_{uu}}{|G_k|^2 S_{m_k m_k} + S_{n_k n_k}} \right)^{-1}. \tag{30}$$

---

[1] From [3], if $\mathbf{A}$ and $\mathbf{B}$ are square matrices and $\mathbf{u}$ and $\mathbf{v}$ are column vectors, and $\mathbf{A} = \mathbf{B} + \mathbf{u v'}$ then $\mathbf{A}^{-1} = \mathbf{B}^{-1} - \lambda \mathbf{y z'}$, where $\mathbf{y} = \mathbf{B}^{-1} \mathbf{u}, \mathbf{z'} = \mathbf{v' B}^{-1}$ and $\lambda = (1 + \mathbf{z' u})^{-1}$.

3.2.2. Generalizing the output channel

Since any of the $q + 1$ channels under consideration can be selected as the output channel, the results above can be generalized to let any of the channels be the output and the remaining channels form the inputs. If the output channel is defined as x_j, and the q input channels as $\{x_i, i \in \mathbf{i}\}$, where $\mathbf{i} = \{1, \dots, q + 1, i \neq j\}$, the results for the optimum transfer functions in Equation (29) can be written as

$$H_{ij} = \frac{G_i^* G_j S_{uu}}{|G_i|^2 S_{m_i m_i} + S_{n_i n_i}} \left(1 + \sum_{k \in \mathbf{i}} \frac{|G_k|^2 S_{uu}}{|G_k|^2 S_{m_k m_k} + S_{n_k n_k}} \right)^{-1}. \tag{31}$$

Similarly, the residual spectra in Equation (30) now becomes the residual of the j channel, and is defined as

$$S_{ee:j} = |G_j|^2 S_{m_j m_j} + S_{n_j n_j} + |G_j|^2 S_{uu} \left(1 + \sum_{k \in \mathbf{i}} \frac{|G_k|^2 S_{uu}}{|G_k|^2 S_{m_k m_k} + S_{n_k n_k}} \right)^{-1}. \tag{32}$$

Since each channel can be selected as the output $j \in \mathbf{j}$, where $\mathbf{j} = \{1, \dots, q + 1\}$, and for each value of j, the optimum system transfer functions and residual spectra can be computed. Note that H_{ij} is defined on $i \in \mathbf{i}$, which are the channels which form the inputs.

3.2.3. Matched channel characteristics approximation

If the anti-aliasing filters are well matched (or can be calibrated to be so) then $G_i = G_j = G$, and the optimum system transfer functions and the residual error expressions will simplify to

$$H_{ij} = \frac{1}{|G|^2 S_{m_i m_i} + S_{n_i n_i}} \left(\frac{1}{|G|^2 S_{uu}} + \sum_{k \in \mathbf{i}} \frac{1}{|G|^2 S_{m_k m_k} + S_{n_k n_k}} \right)^{-1} \tag{33}$$

and

$$S_{ee:j} = |G|^2 S_{m_j m_j} + S_{n_j n_j} + \left(\frac{1}{|G|^2 S_{uu}} + \sum_{k \in \mathbf{i}} \frac{1}{|G|^2 S_{m_k m_k} + S_{n_k n_k}} \right)^{-1} \tag{34}$$

respectively.

3.2.4. Large signal approximation

Since the applied signal u is under user control it should be possible to ensure that the spectral density of the applied signal is much larger than all noise sources, such that $S_{uu} \gg |G|^2 S_{m_i m_i}$ and $S_{uu} \gg S_{n_i n_i}$. Under this assumption the optimum system transfer functions further simplify to

$$H_{ij} = \frac{1}{|G|^2 S_{m_i m_i} + S_{n_i n_i}} \left(\sum_{k \in \mathbf{i}} \frac{1}{|G|^2 S_{m_k m_k} + S_{n_k n_k}} \right)^{-1}, \tag{35}$$

from which it is observed that the optimum system transfer function for each channel is inversely proportional to the combined noise of that channel. Similarly, the residual noise expression now becomes

$$S_{ee:j} = |G|^2 S_{m_j m_j} + S_{n_j n_j} + \left(\sum_{k \in \mathbf{i}} \frac{1}{|G|^2 S_{m_k m_k} + S_{n_k n_k}} \right)^{-1}, \tag{36}$$

from which it is seen that the residual error is the noise of the output channel, plus the parallel combination of the noise of the input channels.

Note that the residual spectrum is always greater than the noise of the present output channel, and that, since the optimum system transfer function for each input channel is inversely proportional to the noise of that input channel, nosier channels are suppressed in the prediction of the output channel, while quieter channels are enhanced.

3.2.5. Amplifier testing with large gain

If the acquisition channel gain is large, such that $|G|^2 S_{m_i m_i} \gg S_{n_i n_i}$, then

$$H_{ij} = \frac{1}{S_{m_i m_i}} \left(\sum_{k \in \mathbf{i}} \frac{1}{S_{m_k m_k}} \right)^{-1} \tag{37}$$

and

$$S_{ee:j} = |G|^2 \left[S_{m_j m_j} + \left(\sum_{k \in \mathbf{i}} \frac{1}{S_{m_k m_k}} \right)^{-1} \right], \tag{38}$$

and the amplifier noise sources are dominate in the optimum system transfer function and residual expressions.

3.2.6. A/D converter testing with small gain

Conversely, if the acquisition channel gain is small, so that $|G|^2 S_{m_i m_i} \ll S_{n_i n_i}$, then

$$H_{ij} = \frac{1}{S_{n_i n_i}} \left(\sum_{k \in \mathbf{i}} \frac{1}{S_{n_k n_k}} \right)^{-1} \tag{39}$$

and

$$S_{ee:j} = S_{n_j n_j} + \left(\sum_{k \in \mathbf{i}} \frac{1}{S_{n_k n_k}} \right)^{-1}, \tag{40}$$

and the converter noise dominates in the optimum system transfer function and residual expressions.

3.3. Determining the channel noise sources from the residual spectra

To determine the individual converter noise of each channel in terms of the directly measurable residual error signals a solution to Equation (36) is required. Assuming that the residual spectrum of each channel has been calculated, with the remaining channels composing the inputs, it is possible to establish a set of nonlinear equations which can be solved for the individual channel noise using a constrained nonlinear least squares optimization procedure.

To demonstrate the situation, consider the case where the gain is small and the converter noise is dominate and four A/D converters sample the same signal, so that $q = 3$ in the above expressions. (This discussion could be performed equally well with combined noise

or the amplifier noise.) Using the coherent removal technique the residual spectrum for each channel can be determined, such that the quantities $(S_{ee:1}, S_{ee:2}, S_{ee:3}, S_{ee:4})$ are known. Applying the approximation given in Equation (40), the residual error spectra of each channel can be expressed in terms of the individual converter noise for each channel as:

$$
\begin{bmatrix} S_{ee:1} \\ \\ S_{ee:2} \\ \\ S_{ee:3} \\ \\ S_{ee:4} \end{bmatrix} = \begin{bmatrix} S_{n_1 n_1} + \left(\dfrac{1}{S_{n_2 n_2}} + \dfrac{1}{S_{n_3 n_3}} + \dfrac{1}{S_{n_4 n_4}} \right)^{-1} \\ S_{n_2 n_2} + \left(\dfrac{1}{S_{n_1 n_1}} + \dfrac{1}{S_{n_3 n_3}} + \dfrac{1}{S_{n_4 n_4}} \right)^{-1} \\ S_{n_3 n_3} + \left(\dfrac{1}{S_{n_1 n_1}} + \dfrac{1}{S_{n_2 n_2}} + \dfrac{1}{S_{n_4 n_4}} \right)^{-1} \\ S_{n_4 n_4} + \left(\dfrac{1}{S_{n_1 n_1}} + \dfrac{1}{S_{n_2 n_2}} + \dfrac{1}{S_{n_3 n_3}} \right)^{-1} \end{bmatrix}. \tag{41}
$$

This nonlinear set of equations can be iteratively solved to determine $(S_{n_1 n_1}, S_{n_2 n_2}, S_{n_3 n_3}, S_{n_4 n_4})$. It is noted that the residual spectra can be used as the initial estimate for the converter noise and that the solutions are constrained such that $S_{II} < S_{n_j n_j} < S_{ee:j}$, where S_{II} is the spectrum of the ideal converter. For $q \geq 2$ this procedure was observed to converge quickly. It should be noted that the matrix does become singular for $q = 1$, which represents the single-input single-output case, which was examined separately in [19].

3.4. Effective number of bits

The most intuitive measure of the quality of an A/D converter is the effective number of bits (ENOB). An A/D converter may provide N digitized bits but the number of bits which are actually *good*, is what is of interest. For an N-bit A/D converter with a voltage range of V_R the device's achievable resolution is $Q = V_R / 2^N$. The effective number of bits is defined as

$$
\text{ENOB} = N - \log_2 \left(\frac{\sigma_n^T}{\sigma_I} \right) \quad \text{(bits)}, \tag{42}
$$

where σ_n^T is the rms value of the total noise of the device under test and σ_I is the rms level of the ideal quantization noise. Inspecting Equation (42), it can be seen that ENOB is a ratio comparing the noise of the device under test to that of an ideal device. Since the ideal quantization noise is well approximated to be a uniformly distributed random variable, its rms level is given as

$$
\sigma_I = \frac{Q}{\sqrt{12}} \quad \text{(V)}. \tag{43}
$$

Determining σ_n^T (the single unknown in Equation (42)), for various operating conditions, forms the basis of nearly all A/D converter testing procedures. For a given sampling rate f_s, the one-sided spectral density of the ideal converter is constant with a value given as

$$
S_{II} = \frac{2}{f_s} \sigma_I^2 = \frac{Q^2}{6 f_s}. \tag{44}
$$

When the multiple channel coherent removal method is applied to A/D converter testing, it is possible to calculate the residual spectra of each channel, compute the converter noise spectra

using the approach described in Section 3.3, and then compute the rms level of the noise σ_n, by integrating the converter noise spectra using Parseval's theorem, such that

$$\sigma_n^2 = \frac{f_s}{P} \sum S_{nn}. \tag{45}$$

To avoid confusion with the ENOB definition, we shall define the number of coherent bits (for an A/D converter) as CB where

$$CB = N - \log_2\left(\frac{\sigma_n}{\sigma_I}\right) \quad \text{(bits)}. \tag{46}$$

which is analogous to ENOB but based on the noise estimated using the coherent removal process.

4. Measurement examples

### 4.1. Multiple channel data acquisition setup

To investigate how the multiple coherence function can be used to dynamically test multiple amplifiers and A/D converters a 4-channel data acquisition system was created using two series of amplifiers as shown in Fig. 4. The Series A amplifiers provide 60 dB of gain and 0.1 Hz ac coupling, while the Series B amplifiers have unity gain, 0.1 Hz ac coupling and a 8-th order Chebyshev low pass filter with a 512 Hz corner frequency.

The amplifiers are a general purpose post amplifier known as the RPA designed (in the early 2000's) for measuring EM signals in the sub-Hertz to 1 kilo-Hertz frequency range. Each channel of the RPA has a differential input which is based on a standard three op-amp instrumentation amplifier design. The RPA is unique in that it uses LTC1150 [13] chopper-stabilized operational amplifiers (op-amps) to eliminate the $1/f$ noise associated with linear op-amps. By modulating the input signal up in frequency, quieter electronics can be used to amplify the signal and then demodulate the signal back to the baseband.

To dynamically test the system a pseudo-random noise source (PRNS) was connected to the input of each of the Series A amplifiers. The PRNS is based on the output of a Linear Feedback Shift Register (LFSR) as described by [7] which is then filtered with a programable raised cosine 10-th order low pass filter. The signal level, cycle rate and clock frequency can be adjusted.

The A/D converters under test are based on an National Instruments (NI) CompactRIO data acquisition system and include four NI 9239 4-channel DAQ modules and one NI 9205 32-channel DAQ module. The NI 9239 modules use 24-bit $\Delta\Sigma$ converters and simultaneously sample the inputs, while the NI 9205 module uses a 16-bit SAR based A/D converter with an inter-channel delay set to 8 μs. (The NI 9205 is capable of sampling up to 250 kHz, using a 4 μs inter-channel delay, but the bit noise increases from 2 LSB, at 8 μs, to 8 LSB.) Note that only eight of the NI 9205 32 channels are used in the following measurement examples.

The total of 24 channels, that are recorded for each measurement example, are arranged such that the first sixteen channels are recorded with the 4 NI 9239 modules and the last eight channels are from the NI 9205. Referring again to Fig. 4, the first NI 9239 module records the input signal (CH1) and three of the Series A amplifier outputs (CH2–CH4). The
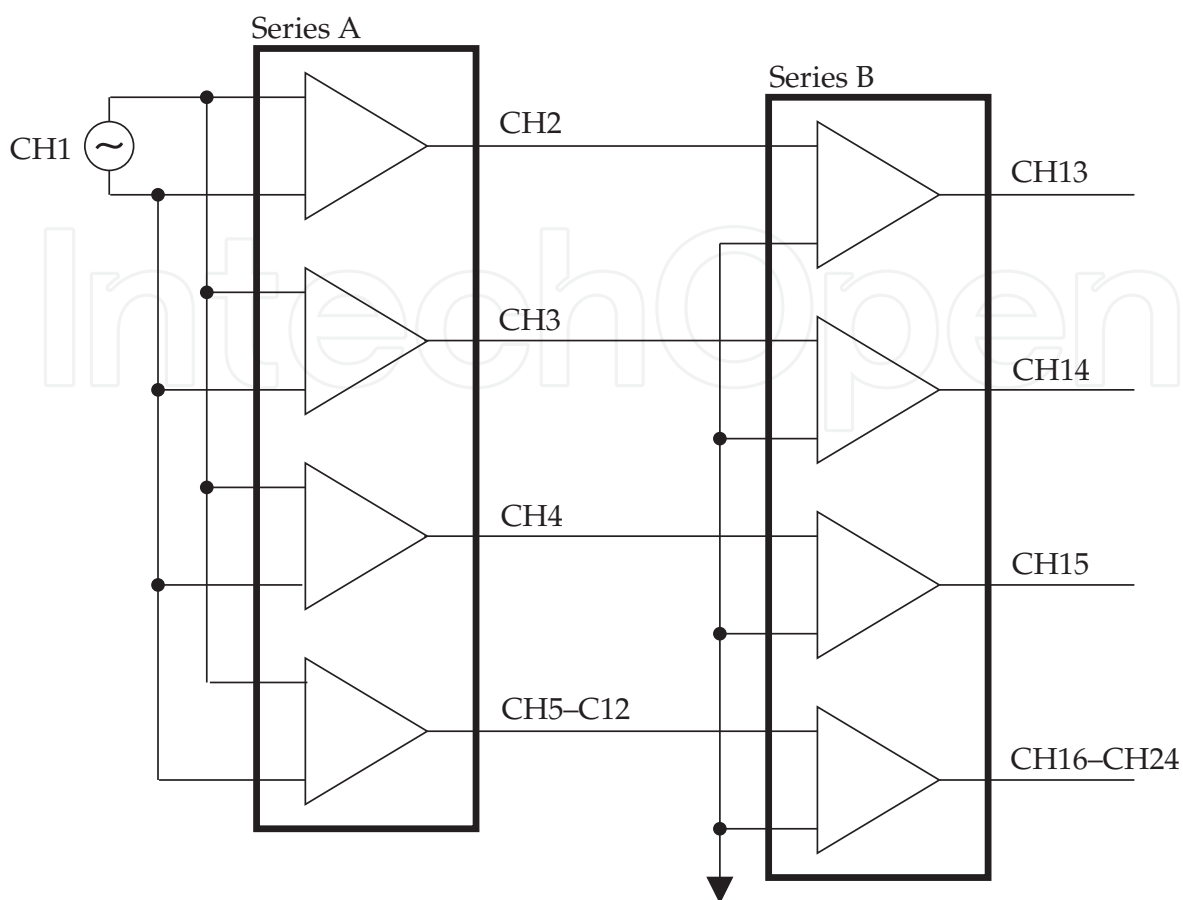
— Amplifiers / Filters —

Series	Gain	Filter
A	60 dB	0.1 Hz 1-st order high-pass
B	0 dB	0.1 Hz 1-st order high-pass and 512 Hz 8-th order low-pass

— A/D Converters —

Channel	Module	Chan.	A/D converter	Sample rate	Simult. sampling
CH1–CH4	NI9239	4	24-bit $\Delta\Sigma$	50 kHz/ch	yes
CH5–CH8	NI9239	4	24-bit $\Delta\Sigma$	50 kHz/ch	yes
CH9–CH12	NI9239	4	24-bit $\Delta\Sigma$	50 kHz/ch	yes
CH13–CH16	NI9239	4	24-bit $\Delta\Sigma$	50 kHz/ch	yes
CH17–CH24	NI9205	32	16-bit SAR	250 kHz	no

Figure 4. Amplifier configuration and channel assignment for the measurement examples.

next two NI 9239 modules (8 channels) record eight copies of the final Series A amplifier output (CH5–CH12). The fourth NI 9239 module records the four outputs of the Series B amplifiers (CH13–CH16), and the NI 9205 records eight copies of the final Series B amplifier (CH17–CH24). Note that the Series B amplifiers provide the anti-aliasing filtering required for the NI 9205 and that the NI 9239 use $\Delta\Sigma$ based A/D converters, which provide their own anti-aliasing.

The four NI 9239 modules share a common sampling clock and the inputs (even between modules) can be considered to be sampled simultaneously. The result of the $\Delta\Sigma$ A/D converter process, however, is not available until 38.4 samples plus 3 µs after the start of the acquisition. Conversely, The NI 9205 provides data from multiple channels asynchronously (i.e. when requested) at rates limited by the inter-channel delay. Coarse synchronization of the two technologies, to within a sample, is accomplished by ignoring an integer number of samples of the NI 9239 at startup. Finer synchronization can be achieved by using filters which delay the signal a fractional number of samples.

4.1.1. Measurement summary

The sampling rate for all the measurement examples is set to 10 kHz and, unless stated otherwise, the following parameters are used for the Welch cross spectral density estimates:

- segment size = 16384
- overlap = 50%
- averages = 256
- Hann data window.

To gain insight into the interpretation of the residual spectra given in Section 3, the 24 channels were recorded for the following three input signals:

1. 16 kHz noise, σ_u=1.6 mV
2. 500 Hz noise, σ_u=3.6 mV
3. 250 Hz sine wave, σ_u=5.3 mV

The precise level of the input signal is not specifically required for the coherent removal process and is given for information purposes. Note that once gained by the Series A amplifiers these mV levels will be V levels at the A/D converters (other than the raw input measurement of CH1). A sample of the data from each channel recorded with the 16 kHz input noise signal is shown in Fig. 5.

The first results to be presented are the transfer functions between the input signal and the output of the Series A and Series B amplifiers. These results are based on the single-input single-output relationships given in Section 2.2, calculated with the wide band noise data set, and include plots of the ordinary coherence function between the input and each of the outputs.

Next the coherent removal process is applied to CH5–CH12 and CH17–CH24 (separately) to calculate the residual spectra of the NI 9239 and the NI 9205 A/D converters; and ultimately the coherent number of bits of both devices. The process is repeated for both noise inputs to investigate how the two different input noise signals effect the two A/D converter types.
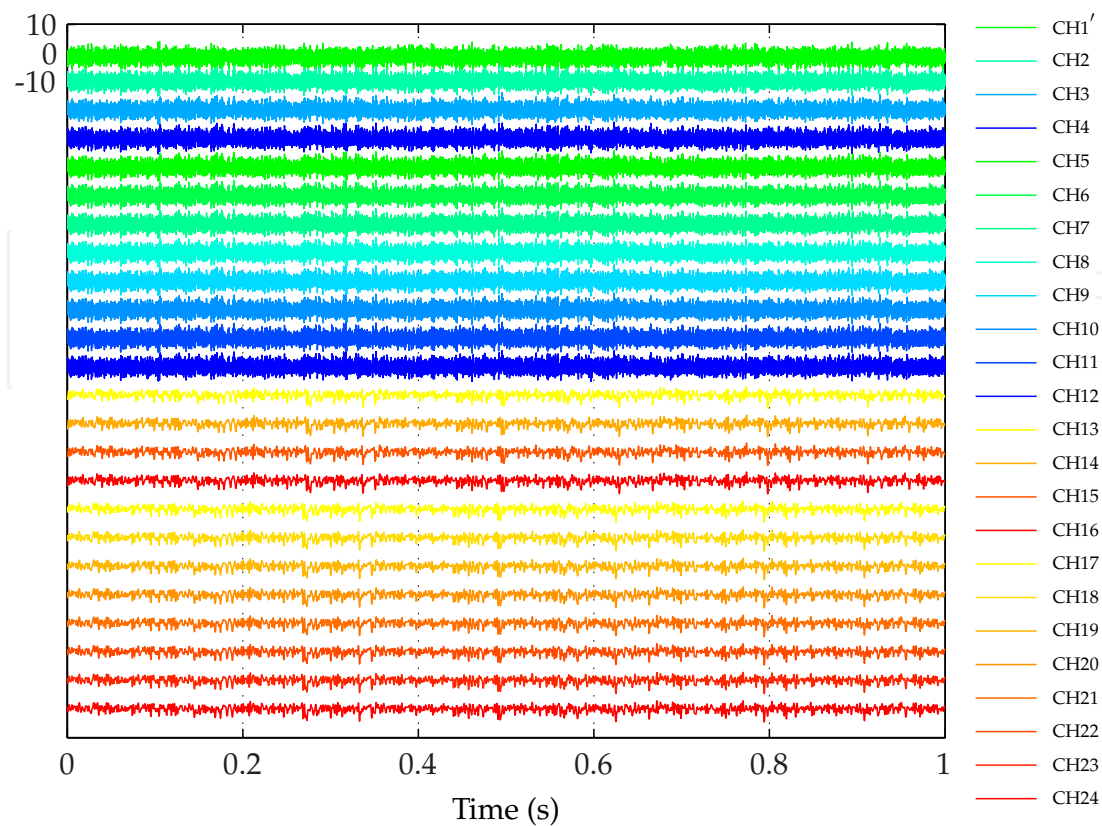
Figure 5. A one second snippet of the raw data recorded with the 16 kHz noise source. The prime on CH1 indicates it has been scaled by 1000, refer to Fig. 4 for channel details.

Next, to investigate the noise of the RPA amplifier the coherent removal process is applied to channels (CH2–CH5) and (CH13–CH16), again for both input noise signals in order to investigate the effect on the RPA amplifier noise (which is based on a chopper-stabilized instrumentation amplifier design).

The last results presented look at the coherent removal process of CH5–CH12 and CH17–CH24 with the sine wave data described above, processed with a Hann window and no window.

4.2. Transfer function measurements

To confirm that each of the amplifiers are operating as specified, transfer function measurements can be calculated using either of the listed noise inputs. The single-input single-output transfer functions of the four Series A amplifiers, namely $G_{1,2}$, $G_{1,3}$, $G_{1,4}$, and $G_{1,5}$, and the transfer functions for the Series B amplifiers, $G_{1,13}$, $G_{1,14}$, $G_{1,15}$, and $G_{1,16}$ were calculated for both input noise signals and little variation in the results were observed.

The magnitude and phase of each of the transfer functions along with the coherence is shown in Fig. 6 for the data collected with the 16 kHz input noise signal. From the transfer functions plots, the gain of the Series A amplifiers is confirmed to be 60 dB, and the 8-th order roll-off and phase response of the Series B Chebyshev filter is evident. As is the custom, γ_{xy} is plotted for the coherence function and it is observed that the coherence is very close to unity, indicating that the output is highly dependent on the input signal. The drop in coherence
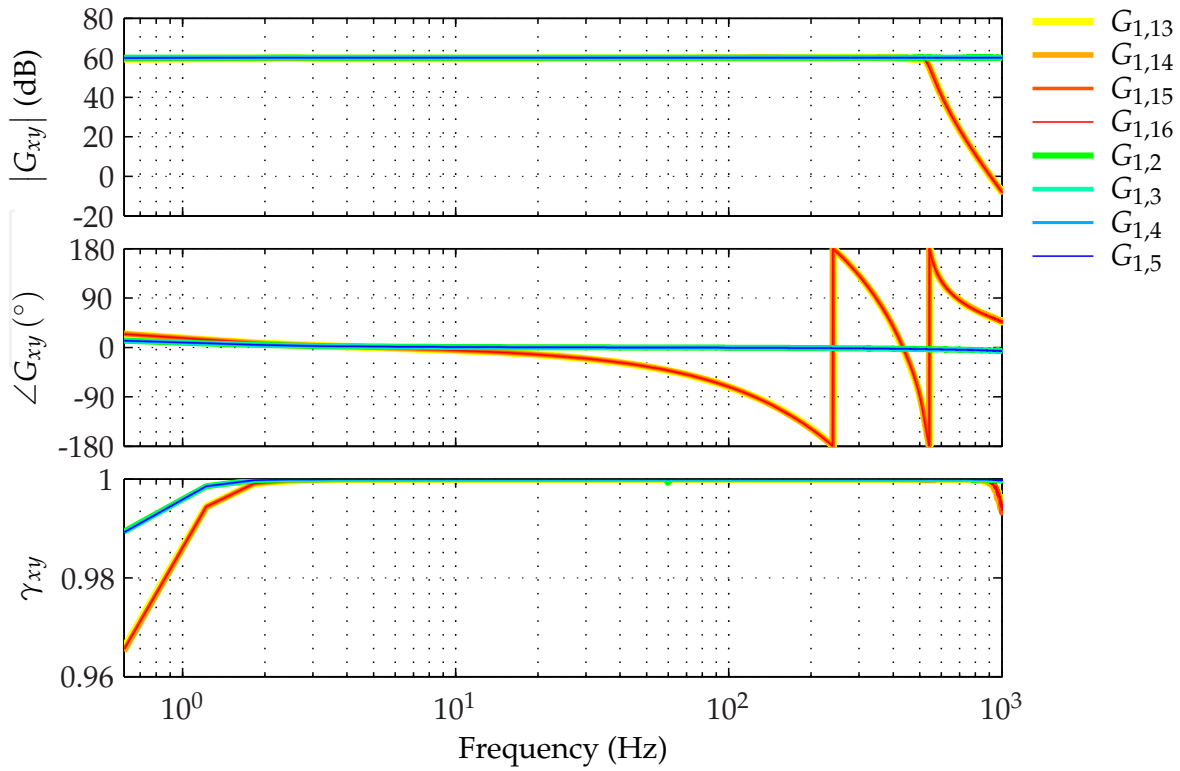
Figure 6. Measured transfer functions (magnitude and phase) and coherence.

below 1 Hz for both, and above 800 Hz for the Series B amplifiers, is due to attenuation of the output signal due to the filtering process. From the results given it is apparent that the amplifiers and filters are performing as specified, and the high level of coherence provides confidence in this assessment.

4.3. A/D converters tests with noise input

We begin the coherent removal examples looking at the residual spectra of CH5–CH12 and CH17–CH24 for the two input noise signals. Fig. 7 shows the input spectra and residual spectra for each channel with the 16 kHz input noise signal, while Fig. 8 shows the results for the 500 Hz input noise signal. For reference the noise floor of an ideal 24-bit and ideal 16-bit device are shown as dashed lines in both figures. We adopt the practice of plotting the input and residual spectra with the same line type and colour, and note that where the curves interact that the input spectra is always greater than the residual spectra.

To compute the individual converter noise spectral densities, the procedure discussed in Section 3.3 is implemented using MATLAB's `fmincon` subroutine, which allows the converter noise of each channel to be calculated at each frequency value. These results are then integrated to obtain the rms level of the converter noise (σ_n), and ultimately the coherent bits (CB), which are tabulated in Table 1.

4.3.1. NI 9239 noise input results

Turning the discussion first towards CH5–CH12, which are the two NI 9239 modules sampling the same Series A amplifier, we observe as expected that all eight input spectra are nearly

input	16 kHz noise σ_u=1.6 V			500 Hz noise σ_u=3.6 V			250 Hz sine wave Hann window			250 Hz sine wave no window		
Chan.	σ_e (µV)	σ_n (µV)	CB	σ_e (µV)	σ_n (µV)	CB	σ_e (µV)	σ_n (µV)	CB	σ_e (µV)	σ_n (µV)	CB
CH5	45.66	42.61	17.05	45.78	42.74	17.04	46.83	43.79	17.01	46.69	43.59	17.02
CH6	45.97	42.96	17.04	46.47	43.50	17.02	46.69	43.63	17.01	46.60	43.49	17.02
CH7	47.06	44.15	17.00	47.32	44.42	16.99	47.13	44.12	17.00	47.69	44.68	16.98
CH8	46.61	43.65	17.01	46.40	43.42	17.02	47.11	44.09	17.00	47.87	44.88	16.97
CH9	46.06	43.06	17.03	45.99	42.97	17.04	47.04	44.02	17.00	47.10	44.03	17.00
CH10	46.48	43.51	17.02	45.86	42.83	17.04	46.70	43.64	17.01	47.68	44.67	16.98
CH11	46.46	43.49	17.02	46.65	43.70	17.01	47.25	44.25	16.99	47.47	44.44	16.99
CH12	46.74	43.80	17.01	46.72	43.77	17.01	47.44	44.45	16.99	47.59	44.57	16.98
CH17	459.6	430.1	13.71	1003.0	940.0	12.58	459.4	429.9	13.71	711.6	679.3	13.05
CH18	460.4	431.1	13.71	993.4	929.6	12.60	459.1	429.6	13.71	631.2	593.3	13.25
CH19	458.7	429.2	13.72	988.5	924.3	12.61	458.7	429.2	13.72	589.9	548.2	13.36
CH20	458.1	428.5	13.72	986.8	922.4	12.61	460.2	430.8	13.71	561.3	516.4	13.45
CH21	457.5	427.9	13.72	991.0	927.0	12.60	460.2	430.7	13.71	568.5	524.5	13.43
CH22	458.8	429.3	13.72	981.0	916.1	12.62	458.0	428.3	13.72	592.9	551.5	13.35
CH23	458.1	428.5	13.72	994.0	930.3	12.60	457.8	428.1	13.72	620.6	581.9	13.28
CH24	459.6	430.2	13.71	1007.8	945.3	12.58	459.1	429.6	13.71	716.3	684.2	13.04

Table 1. Residual spectra levels, converter noise levels, and coherent bits for CH5–CH12 (8 NI 9239 channels) and CH17–CH24 (8 NI 9205 channels) for the three test signals.

identical and that the residual spectra of each channel are approximately equal. It is also noted that the residual spectra are virtually unchanged when the band width of the input noise is changed.

Consistent with the fact that the residuals are unchanged, we see for the 16 kHz input noise signal tabulated in columns 2–4, or the 500 Hz input noise signal tabulated in columns 5–7, nearly identical values for the rms level of the residual, the rms level of the converter noise and the coherent bits. From the table, the NI 9239 achieves about 17.0 coherent bits, at a sample rate of 10 kHz. The consistency of the coherent removal results, for a variety of inputs signals, are a good indicating of the dynamic range of the NI 9239, and its ability to reject signals beyond the Nyquist frequency.

4.3.2. Comments on the input noise spectrum

Closer inspection of the input signal spectrum reveal some interesting facts about the chopper-stabilized instrumentation amplifier design used in the RPA. In order to achieve its improved noise at ultra low frequencies the input signal is chopped (or modulated) at a fixed frequency, which in the case of the RPA is 2.048 kHz. Note that the modulation frequency and its first harmonic are clearly visible in the input spectral densities of Fig. 7.

The RPA design assumes that the input signal is band-limited such that Nyquist theory is satisfied. With the wideband noise source we are clearly violating this requirement, and the
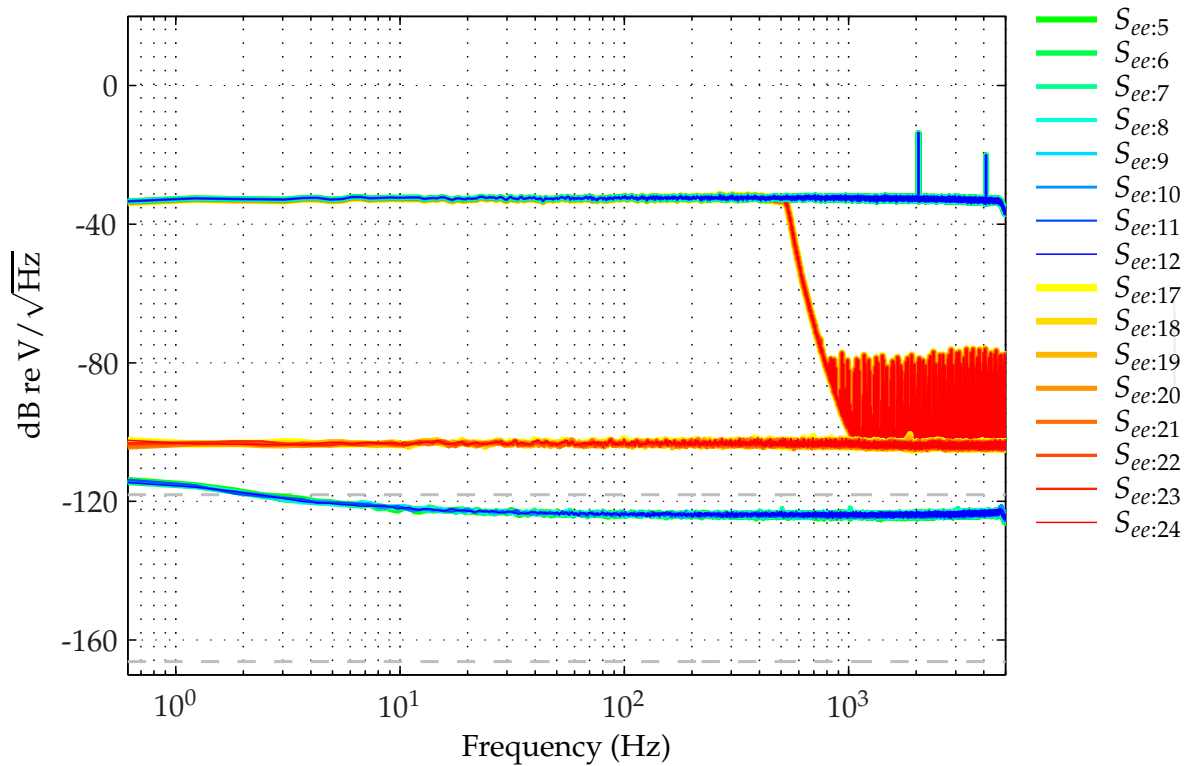
Figure 7. Input and residual spectra for CH5–CH12 and CH17–CH24 with the 16 kHz noise input.

input spectrum is an ensemble of frequencies mixing together due to the chopping process. This mixing is greatly exaggerated when the 16 kHz noise source is used. The net outcome, however, as seen in Fig. 7 is that the spectrum is still flat and harmonics are present at the chopping frequency. When the input noise bandwidth is reduced to 500 Hz, the noise floor of the RPA amplifier (after gain) is now visible for frequencies above $\approx$ 1 kHz as seen in Fig. 8.

In terms of the residual spectra computed for CH5–CH12, which are all measuring the same amplifier output, whatever input signal is used, the residual spectra is limited by the noise of the individual A/D converters and not the amplifier noise present in the signal. We will look at the coherent removal process with the amplifier outputs after discussing the results for the NI 9205, which uses a SAR A/D converter.

4.3.3. NI 9205 noise input results

The importance of using simultaneous sampling to maintain the phase relationship between channels is essential to the coherent removal process. In [19] the introduction of a delay in one of the channels was investigated and was shown to increase the residual spectrum, a result which was consistent with the finding in [4] that the coherence function (as calculated using FFT-based block data methods) has a bias error proportional to the delay between the signals.

How to process the NI 9205 channels presented a bit of dilemma, since absolute synchronization with the NI 9239 modules is achieved by applying a fractional sample delay filter to the NI 9205 channels in order to match the input delay of the $\Delta\Sigma$ A/D converters. And, the design of such a delay filter should in fact minimize the residual spectra of the two channels.
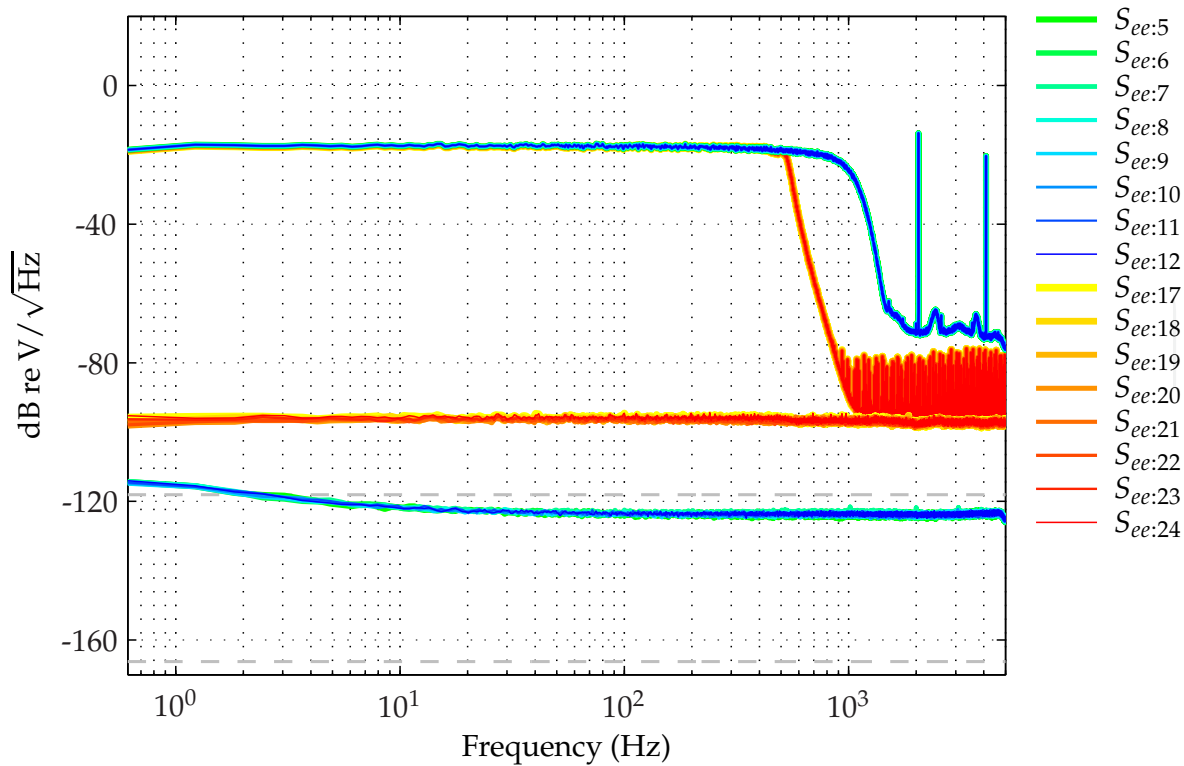
Figure 8. Input and residual spectra for CH5–CH12 and CH17–CH24 with the 500 Hz noise input.

Noting that the bias error in the coherence is proportional to the amount delay, and that the delay between any adjacent channel of the NI 9205 (based on 10 kHz sampling and an 8 μs inter channel delay) represents a delay of only 0.08 of a sample, the decision was made to process the eight NI 9205 channels as a set. It is worth noting that tests done at lower sampling rates would exhibit less inter-channel delay bias.

To simultaneously sample the NI 9205 channels and yield residual spectra that are unbiased by the inter-channel delay, analog sample-hold circuitry could be developed to *sample* the signal and then *hold* the level until the SAR A/D converter is able to read the value. This is in fact how the early coherent removal systems, developed for EM sensing systems, were designed in order to maintain the phase.

Processing data channels CH17–CH24 as a set for the two input noise signals allows us to investigate the residual spectra of the NI 9205 channels for these two test cases. The spectra of the input signals as well as the residual spectra of each channel, are plotted in Fig. 7 and Fig. 8 for the 16 kHz and 500 Hz PRNS tests respectively (alongside the results for the NI 9239). The rms levels of the residuals and converter noise, and the coherent bit values are given in Table 1.

Firstly, it is evident that the residual spectra of the NI 9205 increases when the 500 Hz PRNS source is used. This increase is a result of the fact that the input signal with the narrower band source has a larger signal level resulting in more signal in both the pass band as well as the stop band. It is, however, the increase in the signal level in the stop band that is eventually aliased backed that results in the increase of the residual spectra noise floor. Part of the issue arises from the aliasing artifacts that occur in the input signal due to the chopping process of
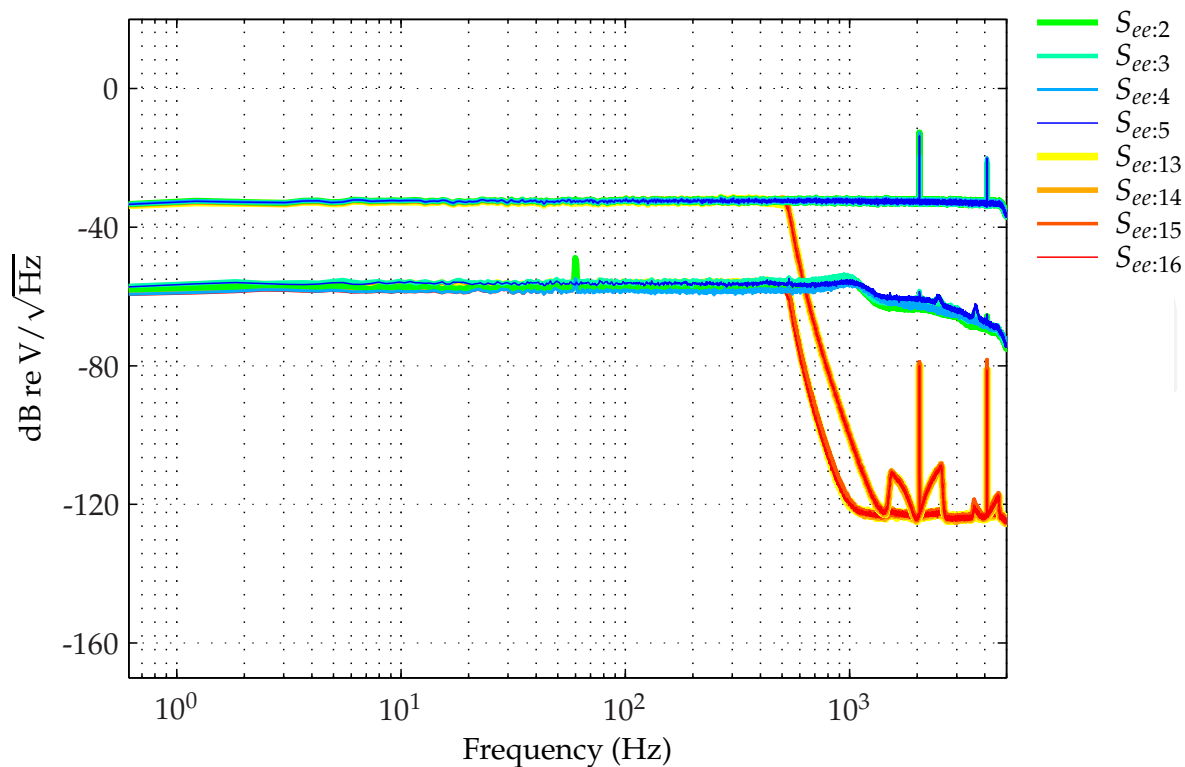
Figure 9. Input and residual spectra for CH2–CH5 and CH13–CH16 with the 16 kHz noise input.

the RPA, which are not adequately removed before the NI 9205 samples the signal. Also, note that the residual spectra of the NI 9205 is flat for frequencies above 1 kHz, indicating that the aliasing artifacts are coherent between channels and removed.

The coherent removal measurements presented here for the NI 9205 are some of the first for a SAR based A/D converter with inter-channel delay. While results are not considered definitive due to the inter-channel delay it does appear that the technique is at least viable as a means to assure a certain level of residual is being achieved. Increasing the number of channels would also help to reduce the residual spectra levels. It is of interest to observe that the first and last channels in the channel list (which are recorded first and last) have the highest residual spectra consistent with the fact that these channels are time-wise the furthest from the other channels.

4.4. Amplifier tests with noise input

To test the coherent removal procedure with amplifier signals we processed channels CH2–CH5 and channels CH13–CH16 each as a separate channel set, for both the input noise signals listed above. Recall that these channels are recorded using the NI 9239 modules and are therefore simultaneously sampled.

The results for each channel set, with the 16 kHz input noise source is shown in Fig. 9. For both of the channel sets, we observe that the noise floor is significantly above the noise level expected for the RPA. The cause is that the chopping process of the RPA is folding incoherent noise back into the frequencies of interest.
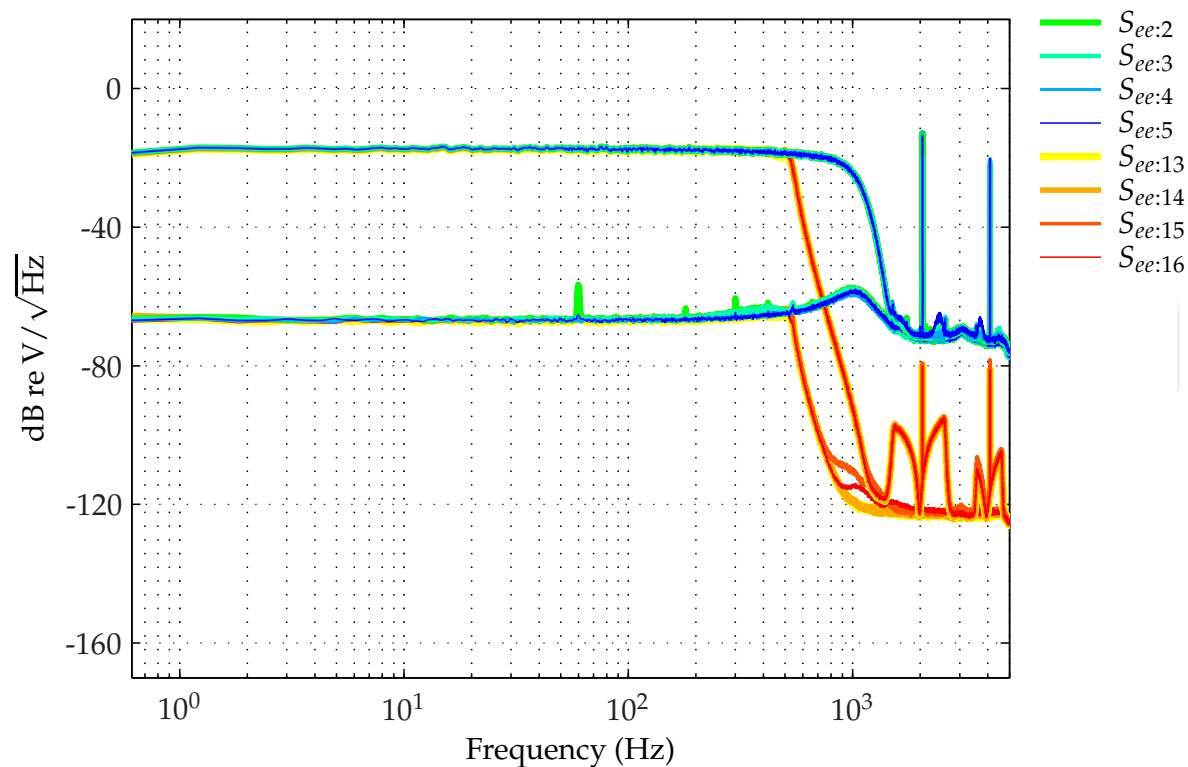
Figure 10. Input and residual spectra for CH2–CH5 and CH13–CH16 with the 500 Hz noise input.

When the 500 Hz input noise signal is used, the input spectrum contains much less out-of-band signal and the RPA residual, as seen in Fig. 10, is closer to the expected level for the RPA.

While the RPA chopping process has complicated the analysis of the amplifier testing presented here, if linear amplifiers had been used, far less variation in the residual spectrum would have been observed with changes in the input signal level and spectrum content.

Similar to the process used to determine the individual converter noise sources, the individual amplifier noise can also be calculated from the residual spectra and if desired the rms level computed. As these are some of the first examples presented for the testing of amplifiers, we conclude the discussion at the calculation of the residual spectra.

In terms of the residual spectra at the output of the Series A amplifiers and the Series B amplifiers the spectra levels are consisted with the operation of the amplifiers and filters for those devices. As an interesting note on the performance improvement with the NI 9239, compare the aliasing artifacts that arose in CH17–CH24, to the spectra for CH13–CH16 which clearly show the chopping harmonics still present in the stop band.

4.5. Sine wave input test

As sine wave inputs are often the test signal of choice for many dynamic testing procedures, it is of interest to test the coherent removal process with a sine wave input and to investigate how changing the data window effects the results. The input and residual spectra for CH5–CH12 and CH17–CH24 with the sine wave signal listed above are shown in Fig. 11, for
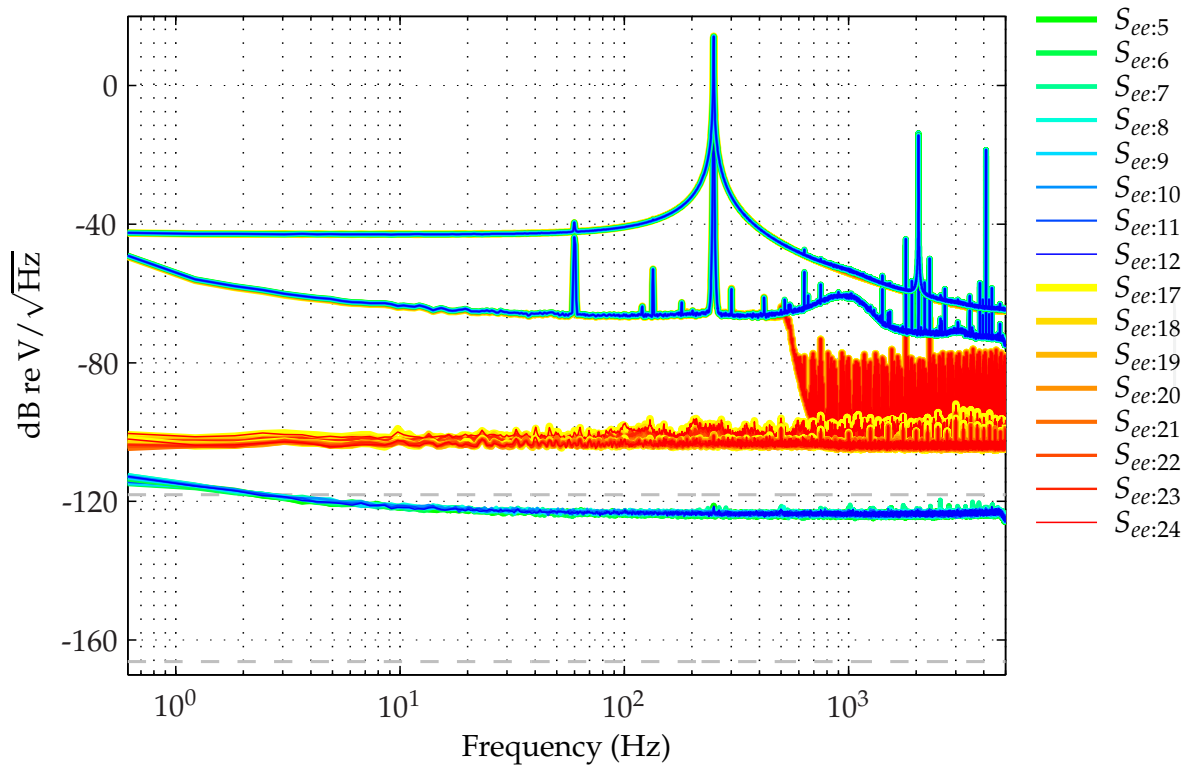
Figure 11. Input and residual spectra for CH5–CH12 and CH17–CH24 with the 250 Hz sine wave input signal processed with no window and the Hann window.

both the Hann window and no window case, and the rms levels of the residual and converter noise, and the coherent bits are given in Table 1.

For the NI 9239 we observe once again that the residual spectra is unchanged from the white noise case, and changing the data window has little effect on this result. For the NI 9205 channels the residual spectra increase slightly when no data window is used, and this is reflected in a 0.7 bit decrease in coherent bits. Why the results are better with the Hann window are not entirely clear, but it appears related to the aliasing artifacts that have been introduced due to the RPA chopping process. Exactly how the window shapes the residual spectra also appears to be influencing the residual calculation.

The sine wave used for this test was of poor quality and with the Hann data window the spectrum of the sine wave can be seen to be contaminated with the noise of the RPA amplifier. This noise accounts for some spectral energy in the input throughout the frequency band and assures the coherent removal process is successful. When there is no (or close to no) signal present in a given frequency band the calculation of the coherence can become numerically unstable. This is, in fact, the case for an ultra pure sine wave processed with a data window to highly suppress the sidelobe energy. In this case, applying no data window actually helps to ensure that signal input is present throughout the frequency band because applying no window causes the spectrum to leak significantly into the sidelobes.

Using sine waves to measure the residual spectrum is somewhat analogous to using a single sine wave to measure the entire transfer function frequency response. As with transfer function measurements, the user should use wideband noise signals to try to maximize the coherence between the signals under test for all frequencies of interest.

4.6. Summary

To implement the measurement examples presented, a LabVIEW application was developed to record and analyze the data in real-time. One of the reasons for implementing the entire processing in LabVIEW was to carry out the calculations using extended precision arithmetic. For the results presented, all of the spectral processing was implemented using MATLAB in double precision arithmetic.

Earlier simulations had suggested the use of extended precision would be necessary when using the coherent removal procedure with large channel counts. These same simulations also showed loss of numerical accuracy when the optimum system transfer functions equations are solved using matrix inversion procedures other than the Cholesky decomposition. While this result is still true, under closer scrutiny, and taking care to simulate bit noise with uniformly distributed variables and the amplifier noise sources with gaussian distributed variables, it was in fact possible to simulate results for as many as thirty-two 24-bit channels with 1 bit of noise using double precision arithmetic. Another important aspect, in order to match simulation results, was to use a large number of spectral averages. While extensive simulations have not been performed, a good rule of thumb is to use about ten times the number of channels, for the number of the averages. For the measurement examples presented no more than eight channels are actually processed using the coherent removal process at one time, so the use of double precision arithmetic and 256 averages is sufficient.

One of the perhaps overlooked aspects of the residual spectra interpretation is that the analysis verifies the practise of paralleling acquisition channels to improve noise performance. When the noise of each of the channels are approximately equal, the residual spectral density will simplify to $S_{ee} = S_{nn} + S_{nn}/q$. The second term in the sum, is actually the noise of the best linear predictor v and has q times lower noise than that of an individual channel.

The ability of modern $\Delta\Sigma$ A/D converters, such as those used in the NI 9239, to provide both simultaneous sampling and brick-wall anti-aliasing filtering, are the principle reasons why, the multiple coherent removal technique works so well for this device. Results with the NI 9205 were hampered, by its inability to simultaneously sample the inputs, and difficulties with aliasing of the input spectrum. The results presented with the NI 9205 make it clear the coherent removal process must take account of the anti-aliasing requirements of the devices under test, by filtering the input signal, or by avoiding inputting signal energy beyond the Nyquist frequency.

The material presented here is derived from well-accepted procedures for computing cross power spectral densities, the optimum system transfer functions, and the residual spectrum. For any combination of channel data, the residual spectra can always be calculated, and from this perspective presentation of the residual spectra is provided similar to that of any other accepted measurement, such as the transfer function or the power spectral density. The approach taken here has been not to present the individual channel noise spectra as these quantities are derived from the residuals and are based on interpretation, certainly, however, the temptation exists to do so, because results become specific to a single device, and this is desirable for marketing purposes.

The use of the multiple coherence function for the dynamic testing of data acquisition channels greatly simplifies the setup, and test signal requirements for dynamic testing of data

acquisition channels because any input signal can be used, and depending on the gain, testing can be performed to measure either the amplifier or the A/D converter noise.

Author details

Troy C. Richards
Defence Research and Development Canada – Atlantic, Canada

5. References

[1] Bendat, J. S. & Piersol, A. G. [1971]. *Random Data: Anlysis and Measurement Procedures*, 1 edn, John Wiley and Sons, New York, NY.

[2] Bendat, J. S. & Piersol, A. G. [1980]. *Engineering Applications of Correlation and Spectral Analysis*, 1 edn, John Wiley and Sons, New York, NY.

[3] Beyer, W. H. (ed.) [1982]. *CRC Standard Mathematical Tables*, 26 edn, CRC Press Inc., Boca Raton, FL.

[4] Carter, G. C. [1980]. Bias in magnitude-squared coherence estimation due to misalignment, *IEEE Transactions on Acoustics, Speech, and Signal Processing* ASSP-28(1): 97–99.

[5] Carter, G. C. (ed.) [1993]. *Coherence and Time Delay Estimation*, 1 edn, IEEE Press, New York, NY.

[6] Holtham, P. M. & McAskill, B. [1987]. The spatial coherence of schumann activity in the polar cap, *Journal of Atmospheric and Terrestrial Physics* 50(2): 83–92.

[7] Horowitz, P. & Hill, W. [1989]. *The Art of Electronics*, 2 edn, Cambridge University Press, Cambridge, UK.

[8] *IEEE Standard for Terminology and Test Methods for Analog-to-Digital Converters* [2000].

[9] Kay, S. M. [1993]. *Fundamentals of Statistical Signal Processing: Estimation Theory*, Prentice Hall, Englewood Cliffs, NJ.

[10] Kuwahara, R. H. [1975]. Examples of DREP magnetics group involvement with coherence-function interpretation and analysis, *DREP Technical Memorandum* (75-7).

[11] Marple, S. L. [1987]. *Digital Spectral Analysis with Applications*, Prentice Hall, Englewood Cliffs, NJ.

[12] Marple, S. L. & Kay, S. M. [1981]. Spectral analysis - a modern perspective, 69: 1380–1419.

[13] LINEAR© [2012]. *LTC1150 Zero-Drift Operational Amplifier*, LINEAR Technology, Milpitas, California.
URL: *www.linear.com*

[14] MATLAB © [2011]. *Signal Processing Toolbox - Help Manaul*, The MathWorks, Inc, Natick, Massachusetts.
URL: *www.mathworks.com*

[15] Motchenbacher, C. D. & Connelly, J. A. [1993]. *Low-Noise Electronic System Design*, John Wiley and Sons,, New York, NY.

[16] Oppenheim, A. V. & Schafer, R. W. [1975]. *Digital Signal Processing*, 1 edn, Prentice Hall, Englewood Cliffs, NJ.

[17] Otnes, R., Lucas, C. & Holtham, P. [2006]. Noise suppression methods in underwater magnetic measurements, *Marelec Conference* .

[18] Press, W. H., Teukolsky, S. A., Vetterling, W. T. & Flannery, B. P. [1992]. *Numerical Recipes in FORTRAN 77*, 2 edn, Cambridge University Press, New York, NY.

[19] Richards, T. C. [2006]. Dynamic testing of A/D converters using the coherence function, *IEEE Transactions on Instrumentation and Measurement* 55: 2265–2274.

[20] Richards, T. C. [2008]. Dynamic testing of A/D converters using the multiple coherence function, *IEEE Transactions on Instrumentation and Measurement* 57: 2596–2607.

[21] Welch, P. D. [1967]. The use of fast fourier transform for the estimation of power spectra: A method based on time averaging over short, modified periodograms, *IEEE Transactions on Audio and Electroacoustics* AU-15: 70–73.